Transport and Communications Science Journal

OPTIMISING TORQUE FOR THREE-DISC AFPMSM IN ELECTRIC VEHICLES USING BP_ANN AND ANFIS ALGORITHMS

Nguyen Van Hai, Vo Thanh Ha*

University of Transport and Communications, No 3 Cau Giay Street, Hanoi, Vietnam

ARTICLE INFO

TYPE: Research Article
Received: 28/11/2024
Revised: 05/12/2024
Accepted: 10/01/2025
Published online: 15/01/2025
https://doi.org/10.47869/tcsj.76.1.1

* *Corresponding author*
Email: vothanhha.ktd@utc.edu.vn

Abstract: Designing an optimal torque distribution controller for the three-disc axial flux permanent magnet synchronous (three-disc AFPMSM) optimises performance while ensuring robustness, stability, and adaptability in a real-world condition. This is crucial for maximising the potential of AFPMSM, particularly in a modern application like an electric vehicle and a renewable energy. Thus, a controller compatible with more complex systems in the future is essential. This paper presents a system that combines torque control algorithms based on a back-propagation neural network (BP-ANN) and an Adaptive Neuro-Fuzzy Inference System (ANFIS). The BP-ANN uses a multi-layer structure where the input layer processes factors such as load torque, rotational speed, and stator current, hidden layers model complex nonlinear interactions, and the output layer predicts optimal torque for AFPMSM operation. Training involves minimising the error between predicted and actual torque through gradient descent and iterative adjustments of weights and biases. The ANFIS-based control enhances performance by integrating neural network learning with fuzzy logic to optimise torque output. By leveraging the strengths of both BP-ANN and ANFIS, the system offers a stable, efficient, and adaptable solution for three-disc AFPMSMs. The Matlab/Simulink simulations confirm its effectiveness, showing balanced torque distribution, reduced energy losses, improved drivetrain efficiency, and adaptability to sudden load or road changes, ensuring stability and enhanced dynamic response.

Keywords: Three-Disc AFPMSM Motors, AFPMSM, BP-ANN, ANFIS.

1. INTRODUCTION

Axial flux permanent magnet synchronous motors (AFPMSMs) are now preferred in electric vehicles for improved torque, reduced pulsation, and higher efficiency [1]. Multi-disc AFPMSMs are ideal for heavy-duty vehicles like buses and trucks due to their compact design, high torque and power density, energy efficiency, durability, and integration potential. By optimising coil and magnet arrangement, AFPMSMs achieve greater power density than radial flux motors, especially in multi-disc designs [2]. These offer high torque, benefiting vehicles needing strong starting and acceleration performance [3]. Their compact design suits integrated systems, combining motor, drive, and controller while saving space and boosting performance over wide speed ranges [4]. The thermal management of AFPMSMs contributes to their reliability and operational longevity. Advanced cooling techniques, such as liquid cooling systems integrated directly into the motor structure, efficiently dissipate heat, ensuring performance stability under high loads and extended operational periods [5]. This feature makes them particularly advantageous for applications in heavy-duty vehicles, which often operate under strenuous conditions.

The three-disc AFPMSM has a complex magnetic field, making it challenging to model factors like saturation, loss, and temperature effects [6]. Optimising its energy efficiency is urgent yet tricky. To tackle these challenges, researchers are exploring hybrid modelling techniques that combine finite element analysis (FEA) with analytical methods to capture better the intricacies of the three-disc AFPMSM's magnetic behaviour [7]. These approaches aim to improve accuracy in predicting performance parameters, enabling more precise control strategies [8]. In addition, advanced control methods like DTC or MPC enhance torque management and energy efficiency, meeting complex demands and enabling quick responses [9]. However, multi-disc AFPMSMs face design challenges due to complex magnetic fields and require precise control for optimal torque distribution. Developing accurate mathematical models and advanced integrated control systems remains a focus for researchers [10]. Intelligent control methods, multi-objective optimisation, and precise modelling are essential. Control strategies like ANN, FLC, and ANFIS excel in managing the motor’s nonlinear traits without needing an exact model [11]. FLC uses experience-based rules to adjust torque for unstable systems, which is ideal for dynamic conditions like electric buses, though it may lack precision under extreme fluctuations [12]. Combining FLC with MPC or ANN improves stability [13]. ANN learns from data to optimise motor torque distribution and maintain efficiency in complex systems, but it requires extensive data, high computational power, and increased costs [14]. Based on the literature [15], sliding mode control (SMC) is based on defining a sliding surface and controlling to keep the system's state always on that surface. This control method can self-adjust when the system is subjected to disturbances or load changes. Therefore, this control method effectively reduces the effects of disturbances and sudden load changes. SMC can respond quickly, helping the electric bus operate stably when facing unexpected situations. In addition, SMC can cause chattering in the control signal, requiring additional techniques to minimise this effect. In addition, PID controllers are optimised using intelligent algorithms. These smart algorithms use optimisation algorithms such as Genetic Algorithm (GA) or Particle Swarm Optimization (PSO) to optimise the parameters of the PID controller to find the optimal PID parameters for torque control. GA-PID and PSO-PID can find the best control parameters for various operating conditions, resulting in efficient torque regulation and increased responsiveness. On the downside, the optimisation process can be time-consuming and only sometimes responds well to conditions

that change too quickly or have high nonlinearity [16]. The ANFIS algorithm combines artificial neural networks and fuzzy logic to learn control rules from training data, automatically adjusting torque based on actual operating conditions. The ANFIS algorithm has good learning and adaptability, allowing flexible torque adjustment based on changes in load and speed conditions. ANFIS is suitable for electric buses because it can learn and adapt in real time. However, ANFIS requires a large amount of data for training and a long calculation time, mainly when operating conditions change rapidly [17]. This paper describes the integrated design of a torque distribution control system for three-disc AFPMSMs. The Backpropagation Neural Network (BP-ANN) optimises the torque for each AFPMSM motor, while the ANFIS algorithm manages the torque of a three-disc AFPMSM based on current conditions. During vehicle operation, the controller processes sensor inputs about the vehicle's status and torque requirements. The system continuously monitors and automatically adjusts the torque in real time, ensuring stable and efficient engine performance under various conditions, such as acceleration.

The paper is organised into five parts. Part 1 highlights the need to enhance motor efficiency for industrial demands, focusing on torque control of the AFPMSM three-disc motor as the solution. Part 2 presents the motor's mathematical model, covering its structure, flux, and dynamic equations, with parameters determined through analysis and experiments. Part 3 introduces a control strategy combining neural networks with the ANFIS method to improve accuracy, reduce computation time, and enhance efficiency. Part 4 validates the approach using MATLAB simulations, while Part 5 summarises the findings, suggests AI enhancements, and outlines future research directions.

2. A THREE-DISC AFPMSM MATHEMATICAL MODEL

The stator windings of this motor are chosen to capture the three-stator, double-rotor AFPMSM operation accurate. This facilitates the development of a mathematical model that closely resembles the conventional model used for PMSMs. The mathematical model developed for the three-disc AFPMSM is expressed within the framework of the three-phase stationary coordinate system, which provides a consistent basis for understanding its performance and integrating it with existing systems and technologies [10].

The equation for calculating voltage is as Eq. (1) [10]

$$\begin{cases} u_{d1} = R_{s1} i_{d1} + L_{d1} \dfrac{di_{d1}}{d_t} - \omega_1 L_{q1} i_{q1} \\ u_{q1} = R_{s1} i_{q1} + L_{q1} \dfrac{di_{q1}}{d_t} + \omega_1 L_{d1} i_{d1} + \omega_1 \psi \\ u_{d2} = R_{s2} i_{d2} + L_{d2} \dfrac{di_{d2}}{d_t} - \omega_2 L_{q2} i_{q2} \\ u_{q2} = R_{s2} i_{q2} + L_{q2} \dfrac{di_{q2}}{d_t} + \omega_2 L_{d2} i_{d2} + \omega_2 \psi \\ u_{d3} = R_{s3} i_{d3} + L_{d3} \dfrac{di_{d3}}{d_t} - \omega_3 L_{q3} i_{q3} \\ u_{q3} = R_{s3} i_{q3} + L_{q3} \dfrac{di_{q3}}{d_t} + \omega_3 L_{d3} i_{d3} + \omega_3 \psi \end{cases} \quad (1)$$

Eq. (2) defines the magnetic flux [10]:

$$\begin{cases} \psi_{d1} = L_{d1} i_{d1} + \psi \\ \psi_{q1} = L_{q1} i_{q1} \\ \psi_{d2} = L_{d2} i_{d2} + \psi \\ \psi_{q2} = L_{q2} i_{q2} \\ \psi_{d3} = L_{d3} i_{d3} + \psi \\ \psi_{q3} = L_{q3} i_{q3} \end{cases} \quad (2)$$

The three-disc AFPMSM torque is calculated using the following Eq. (3) [10]:

$$\begin{cases} T_{m1} = \frac{3}{2} p\left[\psi i_{q1} + (L_{d1} - L_{q1}) i_{d1} i_{q1}\right] \\ T_{m2} = \frac{3}{2} p\left[\psi i_{q2} + (L_{d2} - L_{q2}) i_{d2} i_{q2}\right] \\ T_{m3} = \frac{3}{2} p\left[\psi i_{q3} + (L_{d3} - L_{q3}) i_{d3} i_{q3}\right] \end{cases} \quad (3)$$

The torque of the three-disc AFPMSM is rewritten according to the following Eq. (4) [10]:

$$\begin{cases} T_{m1} - T_{L1} - B_{\omega 1} = \frac{j}{p} \frac{d\omega_1}{d_t} \\ T_{m2} - T_{L2} - B_{\omega 2} = \frac{j}{p} \frac{d\omega_2}{d_t} \\ T_{m3} - T_{L3} - B_{\omega 3} = \frac{j}{p} \frac{d\omega_3}{d_t} \end{cases} \quad (4)$$

In equations (1)–(4) R_{s1}, R_{s2}, R_{s3} are three stator resistors and, respectively u_{d1}, $u_{q1}, u_{d2}, u_{q2}, u_{d3}, u_{q3}$ are d-q axis components of the winding voltage vector of stator 1, stator two and stator 3. $i_{d1}, i_{q1}, i_{d2}, i_{q2}, i_{d3}, i_{q3}$ as shaft component d-q of the coil current vector of stator 1, stator two, and 3. $L_{d1}, L_{q1}, L_{d2}, L_{q2}, L_{d3}, L_{q3}$ are the d-q axial components of the coil inductance of stator 1, stator two and stator 3. $\psi_{d1}, \psi_{q1}, \psi_{d2}, \psi_{q2}, \psi_{d3}, \psi_{q3}$ are the *d-q* axis components of the coil flux of stator 1, stator two và stator three. T_{m1}, T_{m2} và T_{m3} are the electromagnetic moment of the stator 1, stator two và stator 3. T_{L1}, T_{L2} and T_{L3} is the load moment of stator 1, stator 2 and stator 3. *J* is the moment of inertia, and *B* is the viscosity coefficient and load torque. Since two stators share the same rotor, it can be roughly considered that when two motor modules are coaxially connected, it is possible to obtain $\omega_{r1} = \omega_{r2} = \omega_{r3} = \omega_r$. Since the three stators drive the same two rotors, the two rotors are coaxially connected to the three stators, so the three-disc AFPMSM is structurally equivalent to three single-stage AFPMSMs coaxially connected. Thus, the reference coordinate systems correspond to three identical stators. The motors corresponding to the three stators can be analysed using the same *d-q* reference coordinate system. Since the three stators are structurally symmetrical, so we have $R_s = R_{s1} = R_{s2} = R_{s3}$. Besides, the three-disc AFPMSM has a uniform air gap $L_q = L_{q1} = L_{q2} = L_{q3}$.

The moment mathematical equation can be rewritten as follows [10]:

$$T_m = T_{m1} + T_{m2} + T_{m3} = \frac{3}{2} N_p \psi f (i_{q1} + i_{q2} + i_{q3}) \quad (5)$$

Where: T_m is the total electromagnetic torque of the motor T_{m1}, T_{m2}, T_{m3} and is the electromagnetic moment of stators 1, 2 and 3. The coils i_{q3} are a component of stator coil current vectors 1, 2 and 3 in the q-axis.

3. TORQUE CONTROL STRUCTURE FOR A THREE-DISC AFPMSM

3.1. Torque control structure

Figure 1 shows the interconnection structure of a three-disc AFPMSM drive system. This system features three independent stator windings, requiring three motor controllers. Conventional electric vehicle controllers can improve the system's efficiency through communication management. The first vehicle controller sends commands to the communication management unit, which assesses the motors' operating states and torque intensity according to predefined control strategies and distributes control signals and torque data to the three motor modules [10].

Figure 2 shows the core of the control strategy: torque estimation, distribution, and feedback. These elements boost efficiency, reliability, and adaptability by accurately estimating demand, allocating torque, and optimising performance in real-time [10].

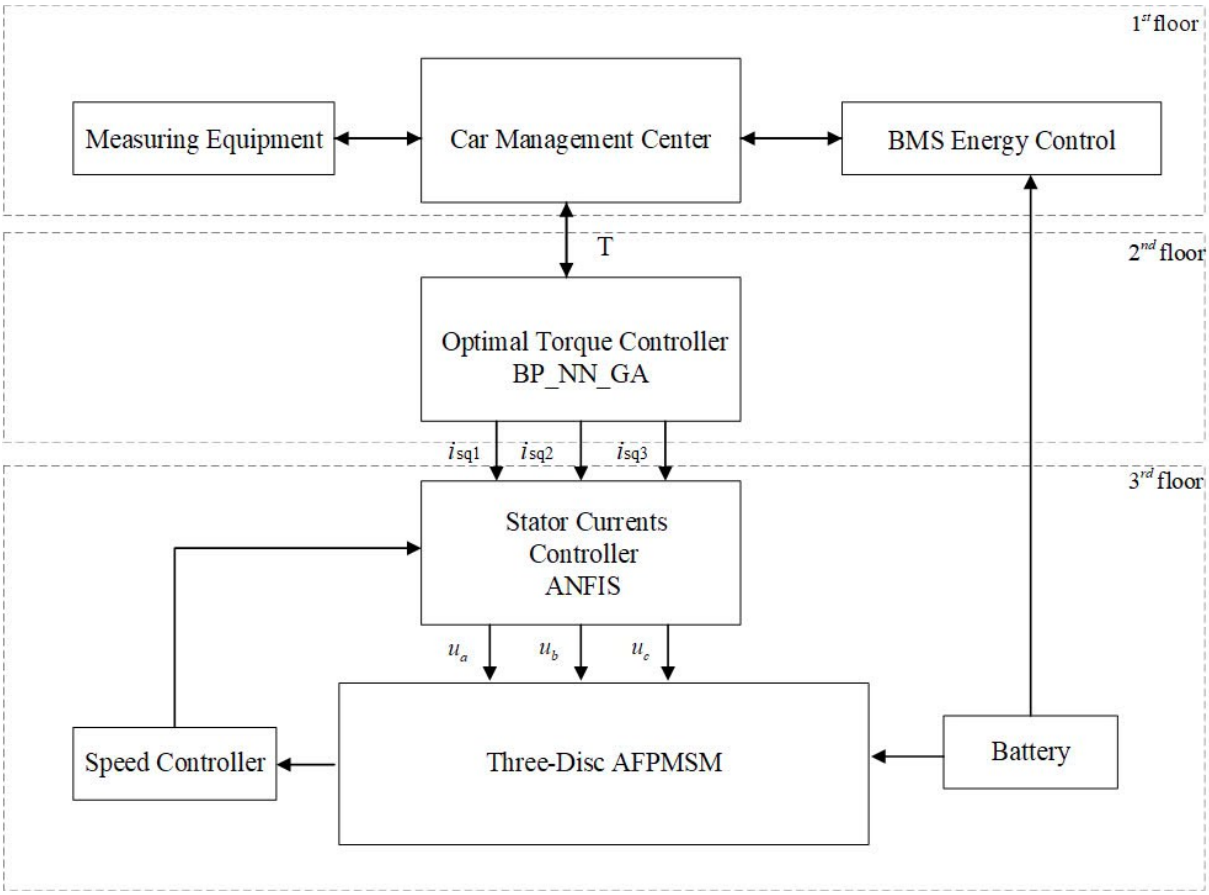

Figure 1. The interconnection structure of a three-disc AFPMSM [10].

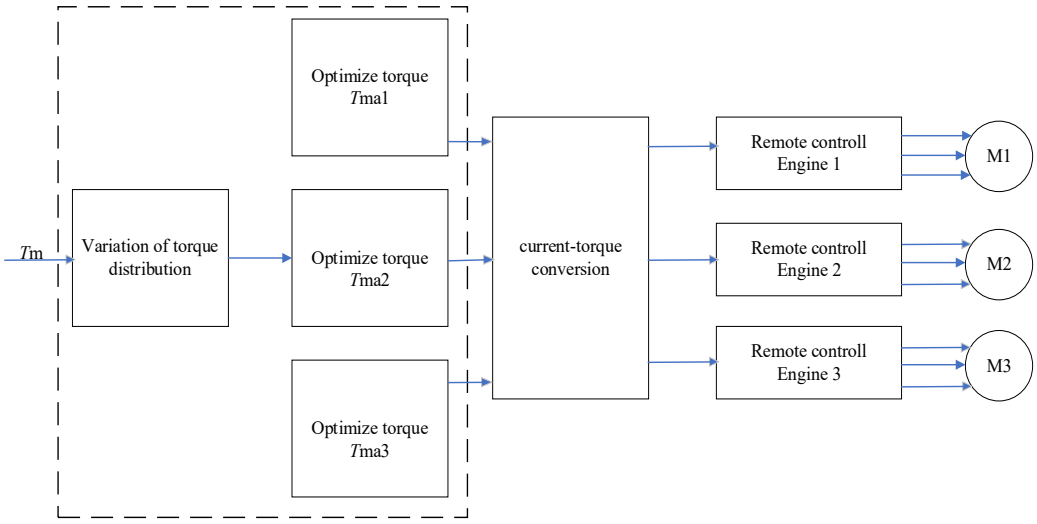

Figure 2. The optimal torque control structure for a three-disc AFPMSM [10].

3.2. A BP-ANN optimal torque control design

The torque of the three-disc AFPMSM is the total of the three independent AFPMSM torques, calculated using Eq. (6) as follows:

$$T = T_1 + T_2 + T_3 \tag{6}$$

The mechanical angular velocity of the motor is ω, and then the output mechanical power of the three sets of motor modules is $T_{\omega 1}$, $T_{\omega 2}$, $T_{\omega 3}$. When the speed is ω and the torque T_1, T_2, T_3 motor modules, a corresponding group of performance, in turn, are η_1, η_2 and η_3 such that $T_1 = a_1 T$, $T_2 = a_2 T$, $T_3 = a_3 T$ where a_1, a_2, a_3 according to [0, 1], and $a_1 + a_2 + a_3 = 1$ The corresponding input power of each group of motor modules are:

$$P_1 = \frac{T_1 \omega}{\eta_1} = \frac{a_1}{\eta_1} T\omega \;\; ; \;\; P_2 = \frac{T_2 \omega}{\eta_2} = \frac{a_2}{\eta_2} T\omega \;\; ; \;\; P_3 = \frac{T_3 \omega}{\eta_3} = \frac{a_3}{\eta_3} T\omega \tag{7}$$

The total input power is calculated as described in Eq. (8):

$$P_i = P_1 + P_2 + P_3 = \left(\frac{a_1}{\eta_1} + \frac{a_2}{\eta_2} + \frac{a_3}{\eta_3} \right) T\omega \tag{8}$$

The total output power is calculated as shown in Eq. (9):

$$P_o = T\omega \tag{9}$$

The performance of the system is expressed as illustrated in Eq. (10):

$$\eta = \frac{P_o}{P_i} = \frac{T\omega}{\left(\frac{a_1}{\eta_1} + \frac{a_2}{\eta_2} + \frac{a_3}{\eta_3} \right) T\omega} = \frac{1}{\frac{a_1}{\eta_1} + \frac{a_2}{\eta_2} + \frac{a_3}{\eta_3}} \tag{10}$$

To improve the system's efficiency, only the total power input needs to be reduced, meaning diminished. Permit $A = \frac{a_1}{\eta_1} + \frac{a_2}{\eta_2} + \frac{a_3}{\eta_3}$. The study minimises a parameter using a three-layer BP-ANN with inputs of torque sum and rotational speed ω. The input layer has two

neurons, the hidden layer four, and the output layer three, corresponding to three parameters a_1, a_2, a_3.

The calculation formula for the hidden layer is calculated by the Eq. (11):

$$S_j = f\left(\sum_{i=1}^{n} X_i \omega_{ij} - \theta_j\right) \tag{11}$$

The *S* function stimulates the output of hidden layer neurons as defined in Eq. (12):

$$f(x) = \frac{1}{1+e^{-x}} \tag{12}$$

The formula for calculating the output of the network according to Eq. (13):

$$Y_k = g\left(\sum_{i=1}^{n} S_j \omega_{jk} - r_k\right) \tag{13}$$

The output of the output layer neurons as described in Eq. (14):

$$g(x) = \frac{1}{1+e^{-x}} \tag{14}$$

The ideal network output and output error are defined in Eq. (15):

$$e_k = Q_k - Y_k \tag{15}$$

The specified error performance indicator function as illustrated in Eq. (16):

$$E_k = \frac{1}{2} e_k^2 \tag{16}$$

For shorter repetition times, the network's weighting factor is adjusted using the slope reduction method, updating coefficients via the negative gradient of the performance index.

$$\triangle w_{jk} = -\eta \frac{\partial E_k}{\partial w_{jk}} = -\eta e_k \frac{\partial Y_k}{\partial w_{jk}} = -\eta e_k Y_k^{'} \tag{17}$$

The equation above is called learning speed and is a preset constant to control the speed of the weight-adjusting connection. It can be seen from the formula of the algorithm to reduce the slope that when the error approaches 0, $\frac{\partial E_k}{\partial \omega_{jk}}$ there will be a tendency towards zero, which will cause the connection weight to no longer be updated. Weight gain is currently the optimal information the neuron learns in the network. The connection weight between the output layer and the hidden layer at time *t+1* as illustrated in Eq. (18):

$$w_{jk}(t+1) = w_{jk}(t) + \triangle w_{jk} \tag{18}$$

The weighted learning algorithm connecting the hidden layer and the input layer as described in Eq. (19):

$$\triangle w_{jk} = -\eta \frac{\partial E_k}{\partial w_{ij}} = -\eta . e_k . \frac{\partial Y_n}{\partial w_{ij}} \tag{19}$$

At t+1, connecting the hidden layer and the weight input layer according to Eq. (20):

$$w_{ij}(t+1) = w_{ij}(t) + \triangle w_{ij} \tag{20}$$

When using a slope reduction algorithm, sometimes the error will oscillate back and forth within a specific range since the η setting is too large. When the η is set too small, the error enters the local minimum score. After hitting the local minimum, the *1w* gradient value

will tend to zero, often called gradient disappearance, making it impossible for the performance function to achieve the global optimal. To prevent errors from going back and forth in a series of fluctuations and slope loss phenomena, the coefficient momentum α (0 < α <1) is added to the method gradient reduction coefficient. Here, α is taken equal to 0.05. As shown in Eq. (21), the amount of weight change becomes.

$$\triangle w(t+1) = -\eta \frac{\partial E_k}{\partial w} + \alpha \triangle w(t) \tag{21}$$

As seen from the equation above, the change in current weight is related to the previous weight shift. If $1w(t)$ > 0, the current weight change is accurate and can be accelerated. If $1w(t)$ < 0, the current weight is prevented from shifting away in the wrong direction. This effectively prevents errors from oscillating and entering local minimums.

3.3. An ANFIS torque control design for a three-disc AFPMSM

The structure of the ANFIS algorithm consists of five layers: the input layer, input member function layer, rule layer, output member function layer, and output layer. A fuzzy interference decision tree classifies data into one of the linear regression models (2^n or p^n) to minimise total squared error (SSE), as shown in Eq. (22):

$$SSE = \sum_i er_i^2 \tag{22}$$

The ANFIS controller for i_d current consists of 2 inputs: the difference (e) between i_d^* and i_d and its integral (Δe). The input signal is dimmed into five triangular inter-triangular functions: negative significant (NB), negative small (NS), equal zero (ZE), positive small (PS), and positive ample (PB). The 5x5 = 25 fuzzy rules combined with the output according to the two-input first-order Surgeon model:

If x_1 *is* A_1 *(NB) and* x_2 *is* B_1 *(NB), then* $f_1 = p_1 e + q_1 \Delta e + r_1$

……

If x_1 *is* A_5 *(PB) and* x_2 *is* B_5 *(PB), then* $f_{25} = p_{25} e + q_{25} \Delta e + r_{25}$

In particular, A_i and B_i are premise fuzzy sets, and p_i, q_i, and r_i are fuzzy design parameters calculated during training (i =1, 2, ... n). The two-input and single-output neuronal fuzzy structure is given as follows:

1^{st} layer: The dimming process occurs; the input signal is dimmed into five inter-triangular functions. For each output value of the first class, we can easily calculate an associated function value denoted by μ

$$O_i^{layer1} = \mu_{Ai}(e) \qquad (i=1, 2, \ldots 5) \tag{23}$$

Where i is the member level of the data set (A1, A2, B1, B2) and is the output of the i^{th} node in layer 1.

2^{nd} layer: Is the weight check of each function. In this class, the input values from the first class are taken and act as optimal functions to represent the data sets of the corresponding input variables. The output of this button is described as follows:

$$O_1^{layer2} = w_1 = \mu_{A1}(e) x \mu_{B1}(\Delta e) \tag{24}$$

3^{rd} layer: Is the rule layer and receives input from the previous layer. Each node (per neuron) in this class performs the conditional matching of the rules. This layer calculates the trigger level of each rule, and the number of layers is equivalent to the number of fuzzy rules. Each node of this class calculates the weight that will typically. Layer 3 nodes calculate the ratio of the trigger intensity of a rule to the sum of all triggering rules:

$$O_i^{layer3} = \overline{w_i} = \frac{w_i}{w_1 + w_2 + ... + w_{25}} \quad (i = 1, 2, \ldots 25) \tag{25}$$

4^{th} *layer:* Fuzzy solution provides output values due to inference of rules. The node output is calculated by multiplying the class 3 output value and the f-rule, respectively:

$$O_i^{layer4} = \overline{w_i}, f_i = \overline{w_i}(p_i e + q_i \Delta e + r_i) \quad (i=1, 2, \ldots 25) \tag{26}$$

5^{th} *layer:* The so-called output layer synthesises all inputs from the 4^{th} layer and converts the fuzzy classification results into sharp values.

$$O_i^{layer5} = \sum_{i=1}^{25} \overline{w_i} f_i = \frac{w_1 f_1 + w_2 f_2 + ... + w_{25} f_{25}}{w_1 + w_2 + ... + w_{25}} \tag{27}$$

4. RESULT SIMULATIONS

Figure 3 shows the optimal torque control for a three-disc AFPMSM in EVs, implemented in MATLAB/SIMULINK. The motor parameters are 160 kW, 3000 rpm, 275 V, six poles, 0.0437 Wb flux, 207 Nm torque, 0.0101 Ω resistance, 0.00024 H *d*-axis, and 0.000297 H q-axis inductance. Two simulations validate the proposed control solution.

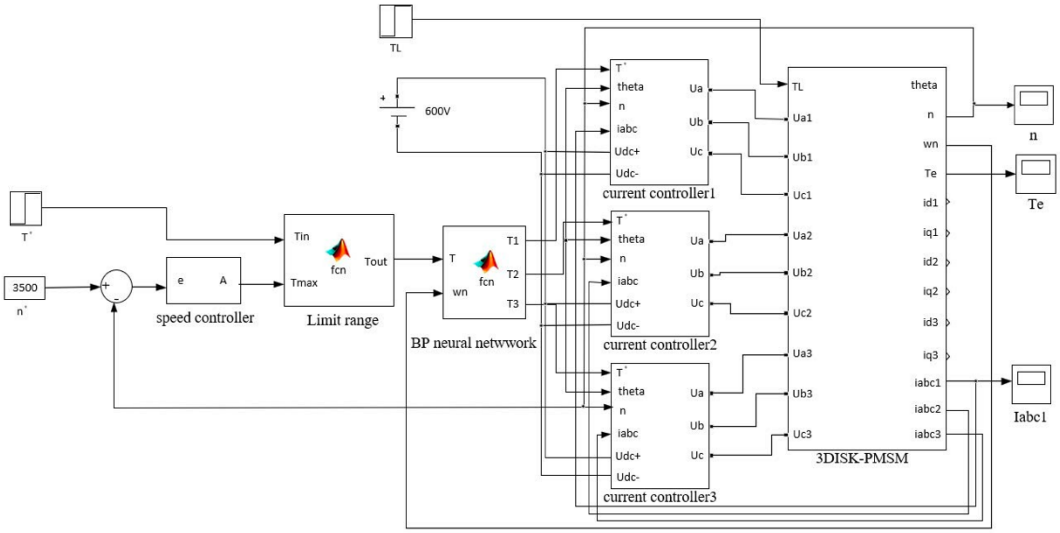

Figure 3. The control structure of the three-disc AFPMSM.

In Fig. 3, the control structure of the three-disc AFPMSM uses a PI speed controller ($K_p = 20.5$, $K_i = 0.992$) optimised for precise speed regulation with minimal overshoot and error. This ensures stability, dynamic performance under load changes, and uniform torque distribution.

Scenario 1: The system and motor accelerate from 0 to 1100 rpm in 5 seconds with

T_L = 20Nm. Figures 4-7 show torque, iq current, 3-phase AC, and speed responses.

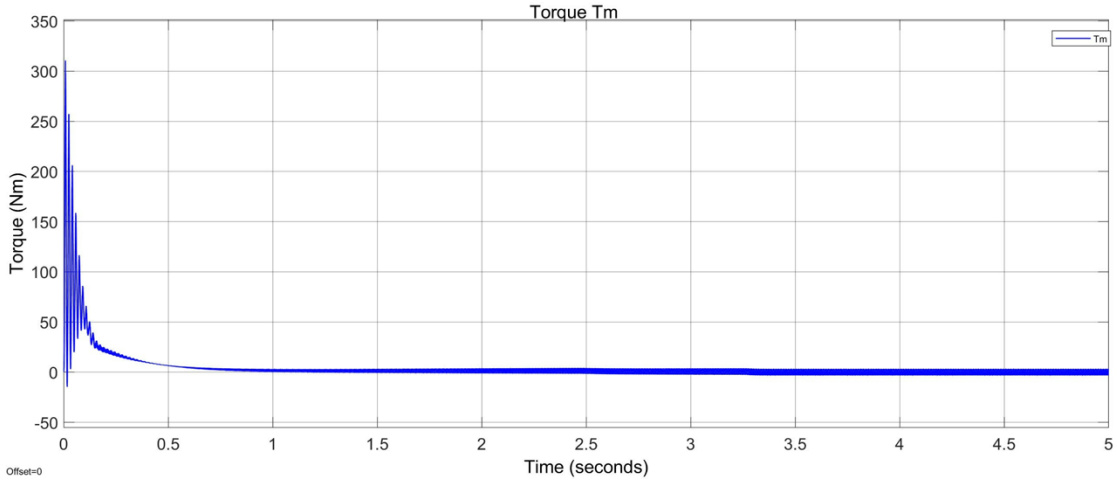

Figure 4. The torque response.

Figure 4 illustrates the motor's torque performance, peaking at 300Nm during startup. Torque increases from 0 Nm to 50 Nm in 0.5 seconds with 8% pulsation. The ANFIS-based controller enhances torque tracking, reducing ripple to below 2%, which is ideal for precision applications requiring smooth operation. Additionally, it reduces overshoot, improves stability, and ensures accuracy and reliability under varying conditions, such as load changes and parameter fluctuations, while minimising energy losses to optimise motor efficiency. By improving torque profiles, reducing harmonic distortion, and enhancing efficiency, the ANFIS-based controller delivers precision, stability, and reliability for advanced motor systems, making it well-suited for demanding applications.

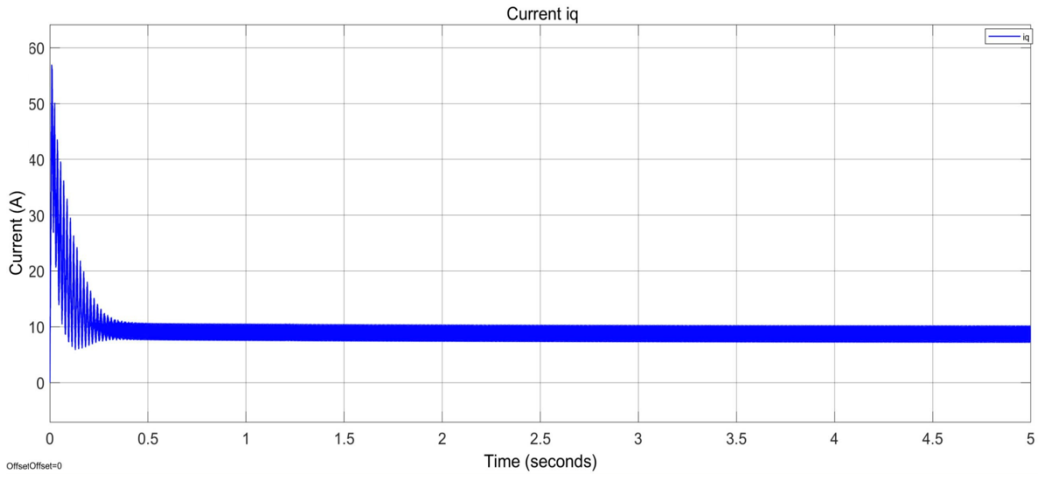

Figure 5. The iq current response.

When the ANFIS system manages iq and reaches 9A, its response is shown in Figure 5, and Figure 6 displays the corresponding three-phase sine waveform. The i_q initially peaks at 55A before stabilising at 9A within 0.5 seconds. A 10% pulse ensures stable torque during this process, highlighting the ANFIS system's efficiency in handling iq dynamics and its rapid response to changes for optimal performance.

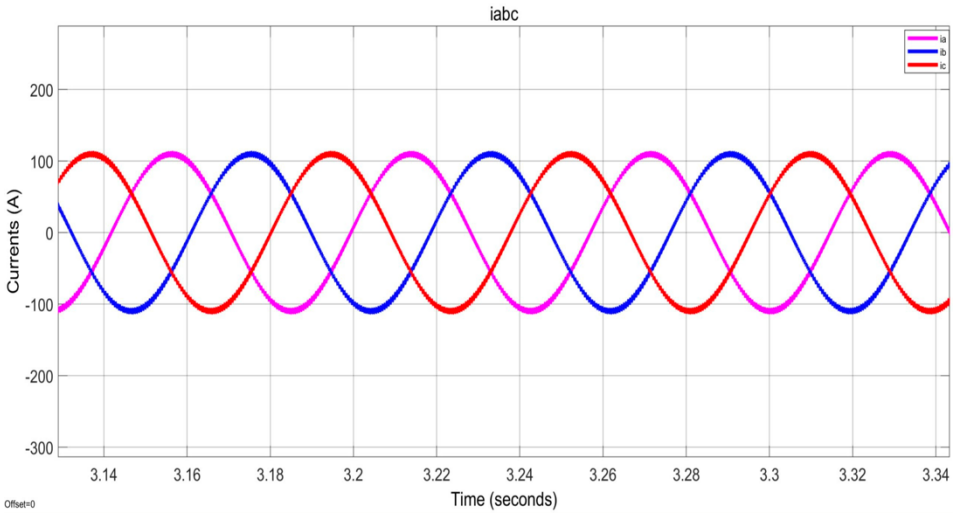

Figure 6. The three ACs' current response.

Figure 6 shows that the motor speed stabilises at 1100 rpm under a 20 Nm load after 0.4s, with no overshoot, demonstrating the effectiveness of the well-tuned speed controller. The smooth, oscillation-free transition to a steady state highlights the control system's robustness, essential for applications demanding precise and stable motor operation where instability could jeopardise performance or safety.

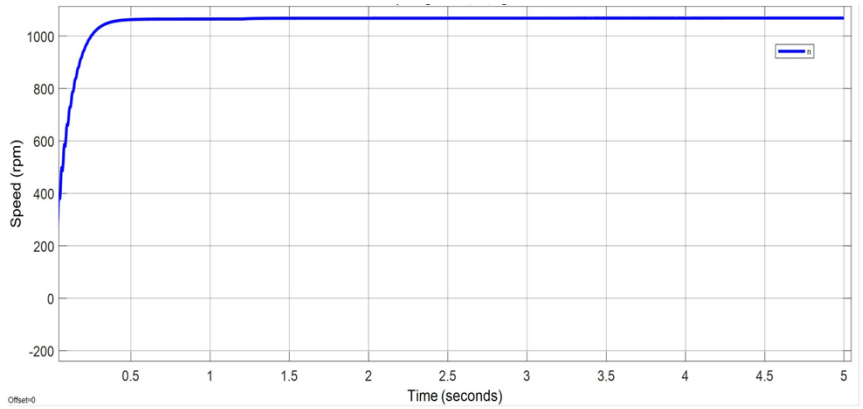

Figure 7. The speed response.

The performance of the three-disc AFPMSM motor is evaluated by analysing the output torque and rotor shaft speed. Its efficiency is calculated using Equation (28) to assess overall effectiveness, providing a comprehensive understanding of the system's capabilities. Figure 8 shows the three-disc AFPMSM performance with optimal torque via neural network control.

$$\eta = \frac{9{,}55 * T * n}{U * I} \tag{28}$$

Simulation scenario one tests motor performance across speeds from 300rpm to 1100rpm (100 rpm steps) and torques from 0 Nm to 200 Nm (20 Nm steps). This covers nine speeds and ten torques, totalling 19 combinations to evaluate performance comprehensively.

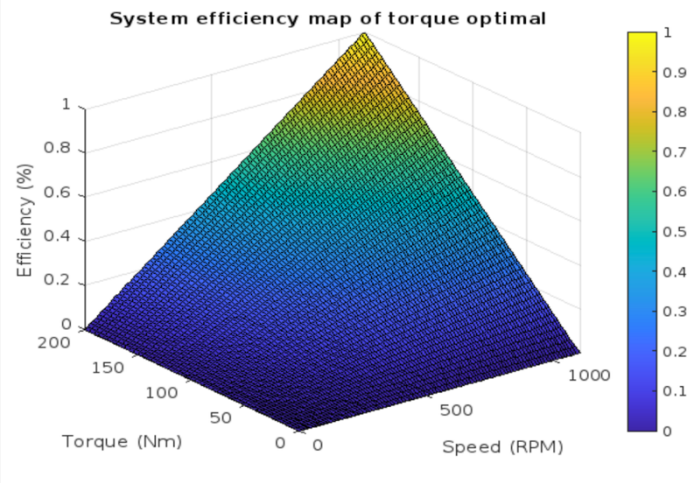

Figure 8. The three-disc AFPMSM performance.

Figure 8 shows that motor efficiency is high within the rated range but drops outside. At 1100 rpm and 200 Nm, efficiency nears 90%, demonstrating the need to optimise operation within design limits. Outside these, energy losses rise due to resistive and mechanical losses. Strategies like torque ripple control and thermal management help maintain efficiency.

Scenario 2: The system operates with a load torque of T_L = 0 Nm and accelerates from 0 rpm to 2300 rpm in 5 seconds.

Figures 9, 10, 11, and 12 detail the results for torque response, i_q current, 3-phase AC, and motor speed, respectively. These figures illustrate the motor's performance and behaviour under the given conditions.

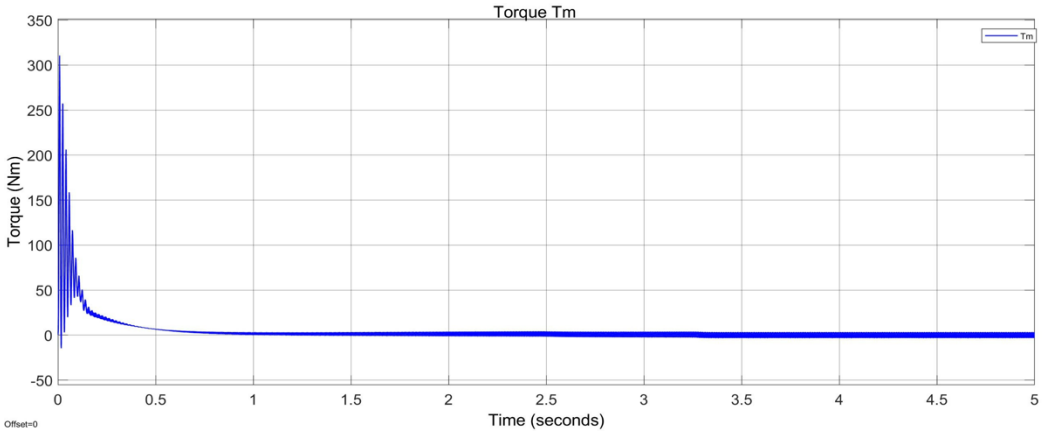

Figure 9. The torque response.

Figure 9 highlights the torque response, showing that the torque reaches a peak value of 300 Nm during the motor's start-up phase. This peak torque is achieved within a time frame of approximately 3.5 seconds. A small torque pulse is observed during stabilisation, amounting to about 3% of the maximum torque.

Applying the ANFIS controller has been highly efficient in optimising the system response. It significantly shortens the time to reach maximum torque and helps the motor start more quickly and efficiently, improving overall system efficiency. The result of the i_q current

response (Figure 10) is similar to case 1. When the i_q current reaches 9A, with both *d*-axis and *q*-axis currents using the ANFIS controller, the waveform of the i_q current is illustrated in Figure 10, and the waveform of the three-phase current is shown in Figure 10. The results show that the i_q current is similar to the torque response: reaching 50A at start-up, then gradually decreasing to 9A in the steady state to maintain torque. The settling time is 3.5 seconds, at which the i_q current still fluctuates by about 10%.

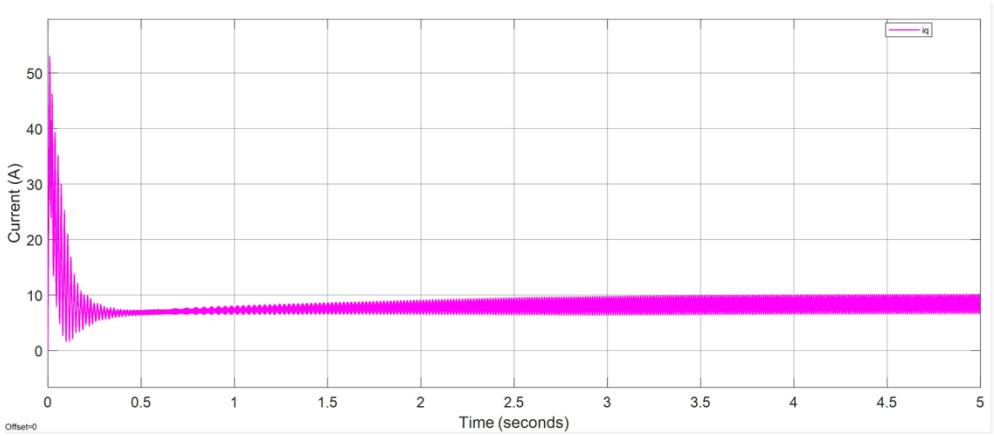

Figure 10. The i_q current response.

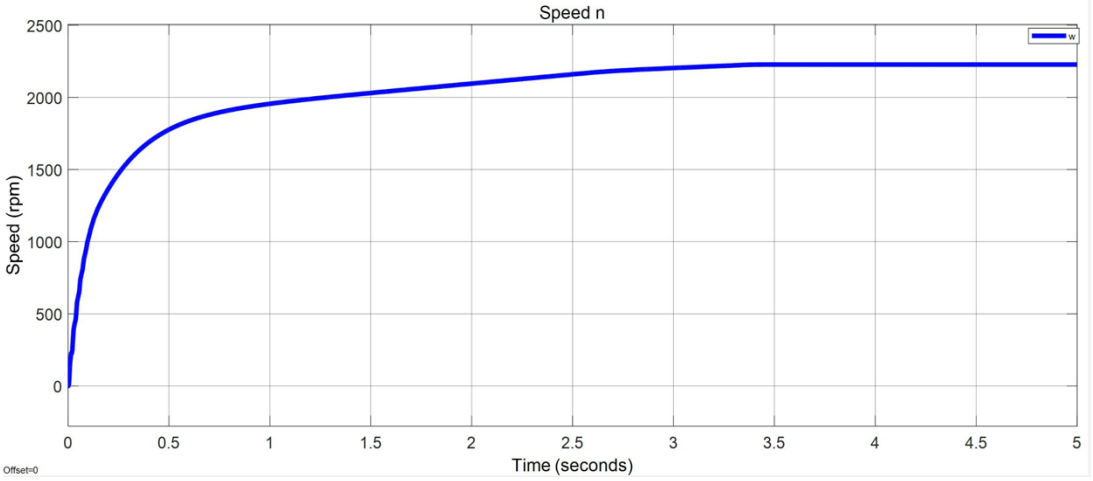

Figure 11. The speed response.

Figure 11 shows that the motor reaches 2300rpm at idle within 3.5 seconds without overshooting, demonstrating the ANFIS controller's efficiency, stability, and precision. Its well-tuned parameters ensure a fast and accurate response while optimising performance. The absence of overshooting enhances stability, reduces mechanical wear, and conserves energy, meeting industrial requirements. The system efficiently manages load changes, maintaining the motor within a safe range. The ANFIS method excels in demanding applications and holds great potential for broader use in modern automation, with future research expected to expand its capabilities.

The efficiency map in Figure 12 illustrates the performance characteristics of the motor system across the tested speed and torque ranges. Motor efficiency peaks within the rated

speed range and decreases outside it. At 2300 rpm and 200 Nm torque, system efficiency reaches 93.3%. At 1500 rpm and 250Nm torque, it slightly decreases to 91.7%. Under lower loads, such as 100 Nm torque and 1800 rpm, efficiency remains at 92.5%. To maximise efficiency, the motor should operate within the optimal speed and load range, where torque and speed are balanced for peak performance. Operating conditions deviating significantly from the optimal range can reduce system efficiency and increase energy losses.

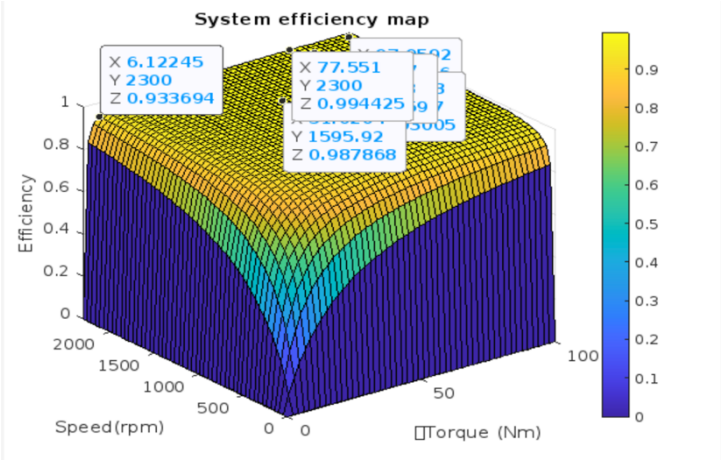

Figure 12. The three-disc AFPMSM motor performance.

5. CONCLUSIONS

The research developed an integrated system for optimal torque distribution and motor control for a three-disc AFPMSM in electric vehicles, equivalent to three coaxial PMSM motors. As confirmed by simulation, a backpropagation neural network algorithm enhances efficiency and durability through optimal torque distribution. The ANFIS current controller meets requirements for settling time and static error. MATLAB/SIMULINK simulations demonstrate the system's stability, anti-interference capability, torque control and current regulation effectiveness. However, the study is limited to MATLAB simulations and requires real-time HIL testing for excellent reliability. Future work will explore intelligent control methods with disturbance observers to reduce reliance on system parameters, enhancing performance and sustainability for the three-disc AFPMSM. The system also offers the potential for advanced energy management strategies in electric vehicles, optimising power consumption and extending battery life. Incorporating real-time adaptive control algorithms could improve performance under varying loads and speeds, while predictive maintenance features leveraging neural network learning could extend operational lifespan and minimise downtime.

ACKNOWLEDGMENT

This research is funded by the University of Transport and Communications (UTC) under grant number T2023-DT- 001TD.

REFERENCES

[1]. Guangyu Zheng, Research on energy saving and emission reduction of urban transportation under low-carbon life, 3rd International Conference on Civil Architecture and Energy Science (CAES 2021), 248 (2021). https://doi.org/10.1051/e3sconf/202124802025

[2]. M. Zhu, X.-Y. Liu, F. Tang, M. Qiu, R. Shen, W. Shu, M.-Y. Wu, Public vehicles for future urban transportation, IEEE Trans. Intell. Transp. Syst., 17 (2016) 3344–3353. https://doi.org/10.1109/TITS.2016.2543263
[3]. X. Sun, C. Hu, J. Zhu, S. Wang, W. Zhou, Z. Yang, G. Lei, K. Li, B. Zhu, Y. Guo, MPTC for PMSMs of EVs with multi-motor driven system considering optimal energy allocation, IEEE Trans. Magn., 55 (2019) 8104306. https://doi.org/10.1109/TMAG.2019.2904289
[4]. Z. Shi, X. Sun, Y. Cai, Z. Yang, G. Lei, Y. Guo, J. Zhu, Torque analysis and dynamic performance improvement of a PMSM for EVs by skew angle optimisation, IEEE Trans. Appl. Supercond., 29 (2019) 1–5. http://hdl.handle.net/10453/131822
[5]. X. Tang, W. Yang, X. Hu, D. Zhang, A novel simplified model for torsional vibration analysis of a series-parallel hybrid electric vehicle, Mech. Syst. Signal Process., 85 (2017) 329–338. https://doi.org/10.1016/j.ymssp.2016.08.020.
[6]. X.-L. Tang, X. Hu, W. Yang, H. Yu, Novel torsional vibration modelling and assessment of a power-split hybrid electric vehicle equipped with a dual-mass flywheel, IEEE Trans. Veh. Technol., 67 (2018) 1990–2000. https://doi.org/10.1109/TVT.2017.2769084
[7]. M. Aydin, M. Gulec, Y. Demir, B. Akyuz, E. Yolacan, Design and validation of a 24-pole coreless axial flux permanent magnet motor for a solar-powered vehicle, Proc. IEEE 22nd ICEM, Lausanne, Switzerland, (2016) 1493–1498. https://doi.org/10.1109/ICELMACH.2016.7732721
[8]. J. Zhao, B. Li, Z. Gu, Research on an axial flux PMSM with radially sliding permanent magnets. Energies, 8 (2015) 1663–1684. https://doi.org/10.3390/en8031663
[9]. A. Hemeida, P. Sergeant, A. Rasekh, H. Vansompel, J. Vierendeels, An optimal design of a 5MW AFPMSM for wind turbine applications using an analytical model, Proc. IEEE 22nd ICEM, Lausanne, Switzerland, (2016) 1290–1297. https://doi.org/10.1109/ICELMACH.2016.7732691
[10]. Jianfei Zhao, li xiao zheng, Shuang Wang, Mini Hua, Research on Deadbeat Current Prediction Vector Control System of Axial Flux Permanent Magnet Synchronous Motor for Electric Bus Based on Efficiency Optimal Torque Distribution Method, (2019). https://doi.org/10.1109/ACCESS.2019.2939759
[11]. B. Nanda, Fuzzy Logic Based Field Oriented Control Of Permanent Magnet Synchronous Motor, International Journal of Electrical Electronics and Data Communication, (2015). https://doi.org/10.18479/ijeedc/2015/v3i8/48350
[12]. D. V.Lukichev, G. L. Demidova, A. Y. Kuzin, A. V. Saushev, Application of adaptive Neuro-Fuzzy Inference System (ANFIS) controller in servo drive with multi-mass object, 2018 25th International Workshop on Electric Drives: Optimization in Control of Electric Drives (IWED), Moscow, (2018) 1-6. https://doi.org/10.1109/IWED.2018.8321388
[13]. W.A. Salem, G.F. Osman, S.H. Arfa, Adaptive Neuro-Fuzzy Inference System Based Field Oriented Control of PMSM & Speed Estimation, 2018 Twentieth International Middle East Power Systems Conference" (MEPCON), (2018) 626-631. https://doi.org/10.11591/eei.v11i4.3818
[14]. Nguyen Van Hai, Vo Thanh Ha, Genetic Algorithm Turned PID Control of AFPMSM for Electrical Vehicle Application, SSRG International Journal of Electrical and Electronics Engineering, 11(2024) 119-128. https://doi.org/10.14445/23488379/IJEEE-V11I2P113
[15]. Vo Thanh Ha, Nguyen Van Hai, Adaptive Neuro-Fuzzy Control of a Single-Sided AFPMSM Motor for Electric Vehicle Applications, SSRG International Journal of Electrical and Electronics Engineering, 11(2024) 118-129. https://doi.org/10.14445/23488379/IJEEE-V11I4P113
[16]. Duy Hoang Dao, Trong Minh Tran, Thanh Ha Vo, Torque Control of an In-Wheel Axial Fux Permanent Magnet Synchronous Motor (AFPMSM) Using Adaptive Neuro-Fuzzy Inference System (ANFIS) for Electrical Vehicles Applications, JTE, 19 (2024). https://doi.org/10.54644/jte.2024.1438
[17]. N. S. Farhan, F. A. Hasan, A. R. D. Humud, Field-oriented control of AFPMSM for an electrical vehicle using adaptive neuro-fuzzy inference system (ANFIS), Engineering and Technology Journal, 39 (2021) 1571-1582. https://doi.org/10.54644/jte.2024.1438